












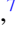





## Fission of $^{180,182,183}\text{Hg}^*$ and $^{178}\text{Pt}^*$ nuclei at intermediate excitation energies

E. M. Kozulin <sup>1,2</sup>, G. N. Knyazheva <sup>1,2</sup>, I. M. Itkis <sup>1</sup>, M. G. Itkis <sup>1</sup>, Y. S. Mukhamejanov <sup>1,3,4</sup>, A. A. Bogachev <sup>1</sup>,  
K. V. Novikov <sup>1,2</sup>, V. V. Kirakosyan <sup>1</sup>, D. Kumar <sup>1,5</sup>, T. Banerjee <sup>1</sup>, M. Cheralu <sup>1</sup>, M. Maiti <sup>6</sup>, R. Prajapat <sup>6</sup>,  
R. Kumar <sup>6</sup>, G. Sarkar <sup>6</sup>, W. H. Trzaska <sup>7</sup>, A. N. Andreyev <sup>8,9</sup>, I. M. Harca <sup>10,11</sup>, A. Mitu <sup>11</sup> and E. Vardaci <sup>12,13</sup>

<sup>1</sup>Flerov Laboratory of Nuclear Reactions, Joint Institute for Nuclear Research, 141980 Dubna, Russia

<sup>2</sup>Dubna State University, 141980 Dubna, Russia

<sup>3</sup>Institute of Nuclear Physics, Almaty, 050032 Kazakhstan

<sup>4</sup>Al-Farabi Kazakh National University, Almaty, 050040 Kazakhstan

<sup>5</sup>GSI Helmholtzzentrum für Schwerionenforschung, 64291 Darmstadt, Germany

<sup>6</sup>Department of Physics, Indian Institute of Technology Roorkee, 247667 Uttarakhand, India

<sup>7</sup>Department of Physics, University of Jyväskylä, FIN-40014 Jyväskylä, Finland

<sup>8</sup>Department of Physics, University of York, York YO10 5DD, United Kingdom


<sup>9</sup>Advanced Science Research Center, Japan Atomic Energy Agency, Tokai, Ibaraki 319-1195, Japan

<sup>10</sup>Facility for Rare Isotope Beams, Michigan State University, East Lansing, Michigan 48824, USA

<sup>11</sup>Horia Hulubei National Institute for R&D in Physics and Nuclear Engineering, Bucharest-Magurele, Romania

<sup>12</sup>Dipartimento di Fisica “E. Pancini” Università degli Studi di Napoli “Federico II,” 80126 Napoli, Italy

<sup>13</sup>Istituto Nazionale di Fisica Nucleare, Sezione di Napoli, 80126 Napoli, Italy

 (Received 1 September 2021; revised 25 October 2021; accepted 24 December 2021; published 6 January 2022)

**Background:** The nature of asymmetric fission of preactinides is not yet understood in detail, despite intense experimental and theoretical studies carried out at present.

**Purpose:** The study of asymmetric and symmetric fission of  $^{180,182,183}\text{Hg}$  and  $^{178}\text{Pt}$  nuclei as a function of their excitation energy and isospin.

**Methods:** Mass-energy distributions of fission fragments of  $^{180}\text{Hg}$ ,  $^{178}\text{Pt}$  (two protons less than  $^{180}\text{Hg}$ ), and  $^{182}\text{Hg}$  (two neutrons more than  $^{180}\text{Hg}$ ) formed in the  $^{36}\text{Ar} + ^{144}\text{Sm}$ ,  $^{142}\text{Nd}$ , and  $^{40}\text{Ca} + ^{142}\text{Nd}$  reactions were measured at energies near and above the Coulomb barrier. Fission of  $^{183}\text{Hg}$  obtained in the reaction of  $^{40}\text{Ca}$  with  $^{143}\text{Nd}$  was also investigated to see if one extra neutron could lead to dramatic changes in the fission process due to the shape-staggering effect in radii, known in  $^{183}\text{Hg}$ .

The measurements were performed with the double-arm time-of-flight spectrometer CORSET.

**Results:** The observed peculiarities in the fission fragment mass-energy distributions for all studied nuclei may be explained by the presence of a symmetric fission mode and three asymmetric fission modes, manifested by the different total kinetic energies and fragment mass splits. The yield of symmetric mode grows with increasing excitation energy of compound nucleus.

**Conclusions:** The investigated properties of asymmetric fission of  $^{180,182,183}\text{Hg}$  and  $^{178}\text{Pt}$  nuclei point out the existence of well-deformed proton shell at  $Z \approx 36$  and a less deformed proton shell at  $Z \approx 46$ .

DOI: [10.1103/PhysRevC.105.014607](https://doi.org/10.1103/PhysRevC.105.014607)

### I. INTRODUCTION

Nuclear fission, discovered over 80 years ago, is still not adequately understood. At present, the fission of preactinide nuclei is a puzzling process. Although the asymmetric fission of preactinides near the  $\beta$ -stability line was known since the end of the 1980s [1], the recent observation of asymmetric fission of the neutron-deficient  $^{180}\text{Hg}$  isotope at ISOLDE [2] provoked the revision of our understanding of this region. It relates to the fact that, whereas in the fission of  $^{180}\text{Hg}$ , the production of  $^{90}\text{Zr}$  fragments with magic neutron numbers  $N = 50$  should be energetically favorable, the formation of fragments with masses 80 and 100 u was observed to be most probable. This is in contrast to the fission of heavy actinides

where the strong shell effects in heavy fragments were found [3,4]. To explain this phenomenon, the new type of asymmetric fission in which the nuclear shells of fragments do not play significant role was assumed. This observation prompted a renewed theoretical [5–12] and experimental [13–20] interest in the fission of neutron-deficient nuclei in the sublead region.

The attempts to explain the new type of asymmetric fission include shell effects in pre-scission configurations associated with dinuclear structures [21] or quadrupole deformed neutron shells in the fragments [9,10,12,22,23] and fissioning nucleus [24]. One of the theoretical studies of the shell effects on fission in the sublead region [7] used the Hartree-Fock approach with BCS pairing correlations. The study concluded

that the mechanisms responsible for asymmetric fission are the same in the preactinide and heavy actinide regions.

The experimental study of fission fragments mass distributions of 14 excited nuclides ( $E^* \approx 30\text{--}60$  MeV) between  $^{176}\text{Os}$  and  $^{206}\text{Pb}$  [16] showed that the proton numbers in the formed fragments (deduced from the simple assumption of the unchanged charge density (UCD) of  $N/Z$  equilibration [25]) are nearly the same for all nuclei, namely,  $Z \approx 36\text{--}37$  for light fragments and  $Z \approx 43\text{--}44$  for heavy ones. For the fission of  $^{205,207,209}\text{Bi}$  [18], it was found that the light fragments have  $Z \approx 38$ , and the heavy fragments have  $Z \approx 45$ . The numbers of neutrons in the fragments change with neutron numbers in the fissioning nucleus. It is to be noted that the proton numbers (not neutron)  $Z = 52$  and  $55$  are responsible for the asymmetric fission of actinides [3,4].

A consistent analysis of the experimental data on low-energy asymmetric fission of neutron-deficient nuclei around lead was performed in Ref. [26] concluding to a leading role played by the light-fragment proton configuration, which is in contrast to the dominance of neutron shells predicted earlier. Detailed theoretical investigation within the microscopic energy density functional framework attribute the experimental observation to shell stabilizations at  $Z = 34$  and  $38$  associated with the more elongated shape ( $\beta_2 > 0.5$ ) for the light fragment with the number of neutrons less than 50 and more compact shape ( $\beta_2 < 0.5$ ) for neutron numbers larger than 50, respectively.

Fission of neutron-deficient  $^{178}\text{Hg}$  formed in the  $^{124}\text{Xe} + ^{54}\text{Fe}$  reaction at the excitation energy of about 34 MeV was studied in Ref. [19]. The isotopic distributions of fragments and their neutron multiplicities were measured using the VAMOS++ spectrometer supplemented with a new detection arm for the coincident measure of the two fission fragments. The analysis of fragment neutron multiplicities performed in Ref. [19] indicates the existence of very elongated proton stabilized configurations for  $Z < 40$ .

In our recent paper [27], the stabilization role of proton numbers at  $Z \approx 36$ ,  $38$ ,  $Z \approx 45$ ,  $46$ , and  $Z = 28/50$  in asymmetric fission of excited preactinide nuclei was observed. In the case of  $^{180,190}\text{Hg}$ , each asymmetric mode is characterized by its own specific total kinetic-energy (TKE) values—the low-energy mode with  $\text{TKE} \approx 128$  MeV for fragments with proton numbers  $Z \approx 36$ , the high-energy mode with  $\text{TKE} \approx 145$  MeV for fragments with  $Z \approx 46$ , and the midenergy mode with  $\text{TKE} \approx 132$  MeV for  $Z = 28/50$ . In the case of  $^{184}\text{Pb}$  fission where the fragments with  $Z = 36$  and  $Z = 46$  are complementary, only the low-energy component ( $\text{TKE} \approx 135$  MeV) was found.

Fission of  $^{178}\text{Pt}^*$  formed in the  $^{36}\text{Ar} + ^{142}\text{Nd}$  reaction has been studied recently in the Japan Atomic Energy Agency [17] using a two-arm time-of-flight (ToF) setup. The low- and the high-energy modes were observed in the TKE distribution of fission fragments at the excitation energy of 50.5 MeV. It was found that the former one corresponds to the narrow symmetric mass distribution, whereas the latter one—corresponds to the asymmetric one with the most probable values of  $M_L = 79$  and  $M_H = 99$  u.

The question arises about multiple modes in asymmetric fission of nuclei neighboring  $^{180}\text{Hg}$ , namely,  $^{178}\text{Pt}$  and

$^{182,183}\text{Hg}$ . They are also interesting for testing shell effects as the relatively well-studied  $^{180}\text{Hg}$  nucleus has two protons more than  $^{178}\text{Pt}$  and two neutrons less than  $^{182}\text{Hg}$ . The other intriguing challenge is to compare the fission observables of  $^{182}\text{Hg}$  and  $^{183}\text{Hg}$  and to see if one extra odd neutron can lead to dramatic changes in the fission process of these nuclei due to the shape-staggering effect known in the ground state of  $^{183}\text{Hg}$  [28].

This paper presents the experimental studies of fission fragments mass and energy distributions from the  $\text{Hg}^*$  and  $\text{Pt}^*$  compound nuclei (CN) formed in the heavy-ion-induced reactions at energies around the Coulomb barrier. In order to investigate the symmetric and asymmetric fission of preactinides in dependence on the excitation energy and proton and neutron numbers of CNs, the mass and energy distributions of fission fragments of  $^{178}\text{Pt}$ ,  $^{182}\text{Hg}$ , and  $^{183}\text{Hg}$  nuclei formed in the  $^{36}\text{Ar} + ^{142}\text{Nd}$  and  $^{40}\text{Ca} + ^{142,143}\text{Nd}$  reactions were analyzed and compared with  $^{180}\text{Hg}$  formed in  $^{36}\text{Ar} + ^{144}\text{Sm}$  measured at the same experiment. Part of the  $^{180}\text{Hg}$  results has already been published [27].

## II. EXPERIMENT

The experiments were performed using the U400 cyclotron at the Flerov Laboratory of Nuclear Reactions, Dubna, Russia. Beams of 158, 169, and 181 MeV of  $^{36}\text{Ar}$  and 172, 192, and 212 MeV of  $^{40}\text{Ca}$  ions struck the layers of  $^{142,143}\text{Nd}$  and  $^{144}\text{Sm}$  235- $\mu\text{g}/\text{cm}^2$  thick deposited on 30- $\mu\text{g}/\text{cm}^2$  carbon backings facing downstream. The energy resolution was  $\sim 1\%$ . Beam intensities on targets were 1 to 2 pnA. The enrichment of the  $^{144}\text{Sm}$ ,  $^{142}\text{Nd}$ , and  $^{143}\text{Nd}$  targets was 93.8%, 99.0%, and 96.5%, respectively.

The binary reaction products were measured in coincidence by the double-arm time-of-flight spectrometer CORSET [29]. Each arm of the spectrometer consists of a compact start detector and a position-sensitive stop detector based on microchannel plates. The angular acceptance of the spectrometer in the reaction plane was  $\pm 10^\circ$  and  $\pm 19^\circ$  for the first and the second arms, respectively. The spectrometer arms were positioned symmetrically with respect to the beam axes at the angles  $\pm 60^\circ$  corresponding to  $90^\circ$  in the center-of-mass (c.m.) system. The angular resolution of the stop detectors was  $0.3^\circ$ , and the time resolution of each arm was about 150 ps. The mass and energy resolutions of the CORSET setup were deduced from the full width at half maximum of the mass and energy spectra of elastically scattered particles. The mass and TKE resolution of the spectrometer under these conditions was  $\pm 2$  u and  $\pm 6$  MeV, respectively.

Data processing assumed standard two-body kinematics [29]. Primary masses, velocities, energies, and angles of reaction products in the c.m. system were calculated from the measured velocities and angles using the momentum and mass conservation laws, assuming that the mass of the composite system is equal to  $M_{\text{target}} + M_{\text{projectile}}$ . Corrections for fragment energy losses in the target material and the detector foils were taken into account. The extraction of the binary reaction channels exhibiting full momentum transfer was based on the analysis of the kinematical diagram (see Refs. [29,30] for details).

TABLE I. The properties of the reactions under study:  $E_{\text{lab}}$  is the beam energy,  $E_{c.m.}/E_B$  is the ratio of energy in the c.m. frame to the Bass barrier [31],  $E_{\text{CN}}^*$  is the initial excitation energy of CN,  $E_{\text{pre}}$  is the energy taken away by prescission neutrons,  $\langle l \rangle$  is the mean angular momentum,  $B(\langle l \rangle)$  is the angular-momentum-dependent fission barrier [32],  $E_{\text{rot}}$  and  $E_{\text{SP}}^*$  are the rotational and excitation energies at the saddle point,  $\sigma_M^{\text{LDM}}$  is a standard deviation of mass distribution, estimated via systematics [33] based on the liquid drop model (LDM),  $\text{TKE}_{\text{Viola}}$  is a total kinetic energy for the symmetric mass split estimated from the Viola systematics [34].

Reaction	CN	$E_{\text{lab}}$ MeV	$E_{c.m.}/E_B$	$E_{\text{CN}}^*$ MeV	$E_{\text{pre}}$ MeV	$\langle l \rangle$ $\hbar$	$B(\langle l \rangle)$ MeV	$E_{\text{rot}}$ MeV	$E_{\text{SP}}^*$ MeV	$\sigma_M^{\text{LDM}}$ u	$\text{TKE}_{\text{Viola}}$ MeV
$^{36}\text{Ar} + ^{142}\text{Nd}$	$^{178}\text{Pt}$	158	1.00	42	2.9	8	12.8	0.2	26.0	9.4	136.0
		169	1.07	51	10.4	24	10.9	2.0	27.7	9.5	
		181	1.15	60	18.1	35	8.7	4.5	28.7	9.6	
$^{36}\text{Ar} + ^{144}\text{Sm}$	$^{180}\text{Hg}$	158	0.97	34	0	8	10.0	0.2	23.8	9.7	142.1
		181	1.12	53	12.0	31	7.1	3.4	30.5	10.3	
$^{40}\text{Ca} + ^{142}\text{Nd}$	$^{182}\text{Hg}$	172	0.97	37	0.0	8	10.6	0.2	26.1	9.9	141.6
		192	1.08	52	11.8	28	8.3	2.6	29.3	10.1	
		212	1.19	68	25.6	45	4.8	6.9	30.7	10.3	
$^{40}\text{Ca} + ^{143}\text{Nd}$	$^{183}\text{Hg}$	172	0.97	39	0.4	8	11.1	0.2	26.9	9.9	141.3
		192	1.08	55	11.7	29	8.6	2.8	29.2	10.3	
		212	1.19	71	23.5	46	5.0	7.0	28.5	10.6	

### III. RESULTS AND DISCUSSION

#### A. Mass-energy distributions of fission fragments

The energy-dependent characteristics for the studied reactions are given in Table I. To obtain the CNs at the lowest possible excitation energies, the measurements were performed near the Coulomb barrier (see Table I). It allowed us to investigate the fission process of the studied nuclei in the excitation energy range of 34–71 MeV. In this case, the prescission neutron and proton emission may take away some part of the initial excitation. The prescission neutron multiplicities were estimated using the systematics [35]. The number of protons emitted before scission calculated with NRV code [36] is, at least, three times less than that of neutrons (one order of magnitude in most cases) and may be neglected in our paper. Therefore, the actual fissioning isotope and its excitation energy may differ from initial CN, especially at the highest excitation energies where the influence of prescission emission is the strongest. Since the influence of dynamic effects on descent from the fission barrier to the scission point is comparatively small for preactinides [7], the fission properties of these nuclei are mainly determined at the saddle point and depend on its excitation energy in the simplest approximation defined as

$$E_{\text{SP}}^* = E_{\text{CN}}^* - B_f(\langle l \rangle) - E_{\text{pre}} - E_{\text{rot}},$$

where  $B_f(\langle l \rangle)$  is the angular-momentum-dependent fission barrier,  $E_{\text{pre}}$  is the energy loss due to prescission neutron emission, and  $E_{\text{rot}}$  is the rotational energy at the saddle point. Since the angular momenta introduced by the Ar and Ca projectiles are relatively large (see Table I), we used a fission barrier for rotating liquid drop [32]. The values of the interaction energies, excitation energies of formed CNs, mean angular momenta of CN calculated with the PACE4 code [37], fission barriers at these  $\langle l \rangle$ s, and excitation energies at the saddle point for the studied reactions are listed in Table I.

Mass-total kinetic energy ( $M$ -TKE) distributions of the primary binary fragments obtained in the  $^{36}\text{Ar} + ^{142}\text{Nd}$ ,  $^{36}\text{Ar} + ^{144}\text{Sm}$ , and  $^{40}\text{Ca} + ^{142,143}\text{Nd}$  reactions leading to the formation of  $^{178}\text{Pt}$  and  $^{180,182,183}\text{Hg}$  isotopes at all measured energies are shown in Fig. 1. In the  $M$ -TKE matrices, the fissionlike products within the contour lines are separated well enough from elastic and quasielastic scattering events. They are characterized by large mass transfer and energy dissipation and can originate from either CN-fission or quasifission (QF) processes.

From the analysis of a large set of experimental mass-angular distributions of fissionlike fragments formed in the reactions with heavy ions [38], it was found that for the composite systems with  $Z_{\text{CN}} = 80$  the threshold value for the QF appearance is  $Z_1 Z_2 = 1450 \pm 100$ . Among the reactions under investigation, the largest value of  $Z_1 Z_2 = 1200$  reached for  $^{40}\text{Ca} + ^{142}\text{Nd}$  is significantly lower than the threshold one. Thus, all studied reactions are favorable for CN formation.

As seen in Fig. 1, at comparable excitation energies the mass-energy distributions are similar for all four reactions. Although at the high energies, their shape is rather typical uniform LDM behavior, at the lowest measured energies, one can see the structures in the  $M$ -TKE matrices.

The mass distributions of fission fragments of excited  $^{178}\text{Pt}$  and  $^{180,182,183}\text{Hg}$  (events inside the contour lines in the  $M$ -TKE distributions in Fig. 1) normalized to 200% are presented in the left panels of Figs. 2–5. The mass distributions are flattopped in the symmetric mass region at high energies and have a pronounced asymmetric component at lowest measured energies. The values of the most probable masses of the light and the heavy fragments are found to be 80 and 100 u for  $^{180}\text{Hg}$  (which is similar to  $^{180}\text{Hg}$  from  $\beta$ -delayed fission of  $^{180}\text{Tl}$  [2]), 81 and 101 u for  $^{182}\text{Hg}$ , 82 and 101 u for  $^{183}\text{Hg}$ , and 82 and 96 u for  $^{178}\text{Pt}$ .

The TKE distributions of fission fragments of excited  $^{178}\text{Pt}$  and  $^{180,182,183}\text{Hg}$  for different mass ranges (symmetric mass split  $A_{\text{CN}}/2 \pm 5$  u, mass range where the maximal yield of

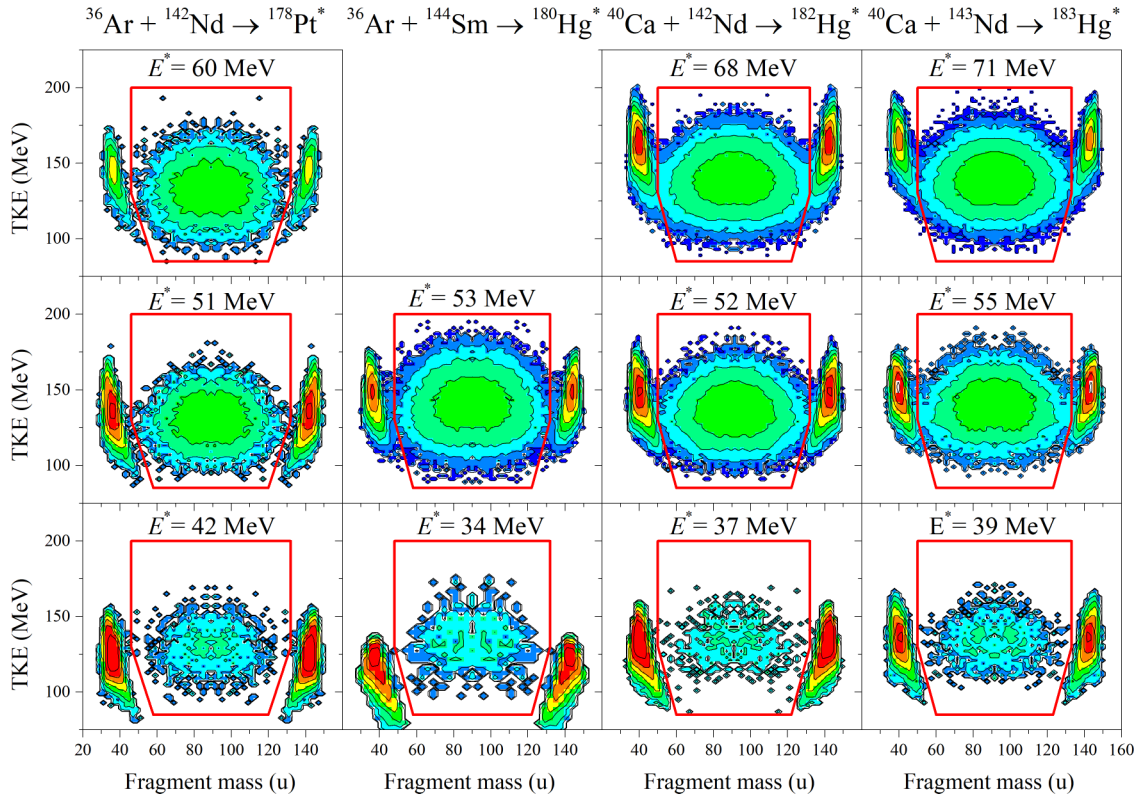


FIG. 1. The mass-energy distributions ( $M$ -TKE matrices) of binary fragments formed in the  $^{36}\text{Ar} + ^{142}\text{Nd} \rightarrow ^{178}\text{Pt}^*$ ,  $^{36}\text{Ar} + ^{144}\text{Sm} \rightarrow ^{180}\text{Hg}^*$ ,  $^{40}\text{Ca} + ^{142}\text{Nd} \rightarrow ^{182}\text{Hg}^*$ , and  $^{40}\text{Ca} + ^{143}\text{Nd} \rightarrow ^{183}\text{Hg}^*$  reactions at energies around the Bass barrier. The events inside the contour lines are fission fragments, and the left and right intense peaks correspond to the scattered beam ions and the recoil target nuclei.

asymmetric modes is found, and very asymmetric fragments with masses 50–70 u) are presented in the right panels of Figs. 2–5.

At the first glance, the mass distributions for all nuclei under consideration consist only from one symmetric and one asymmetric mode. But the TKE distributions have a com-

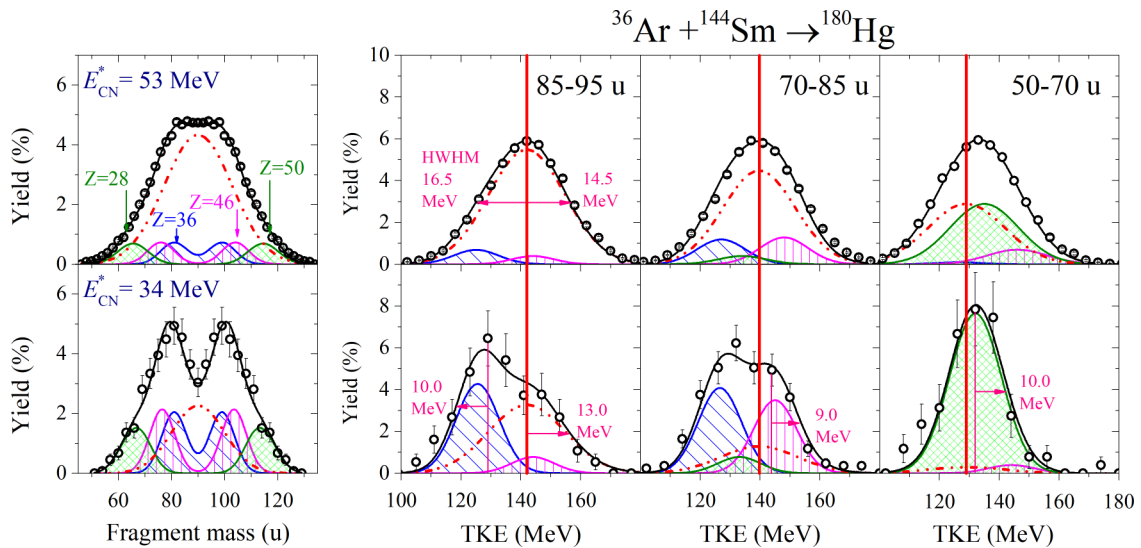
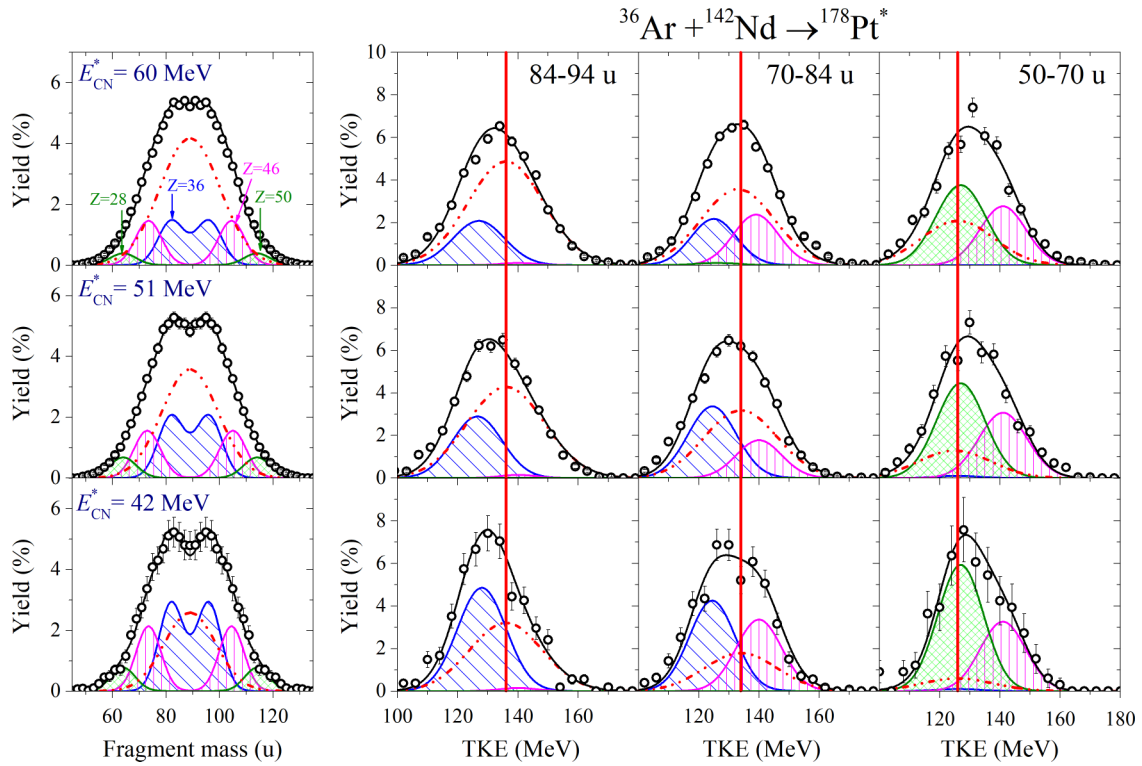
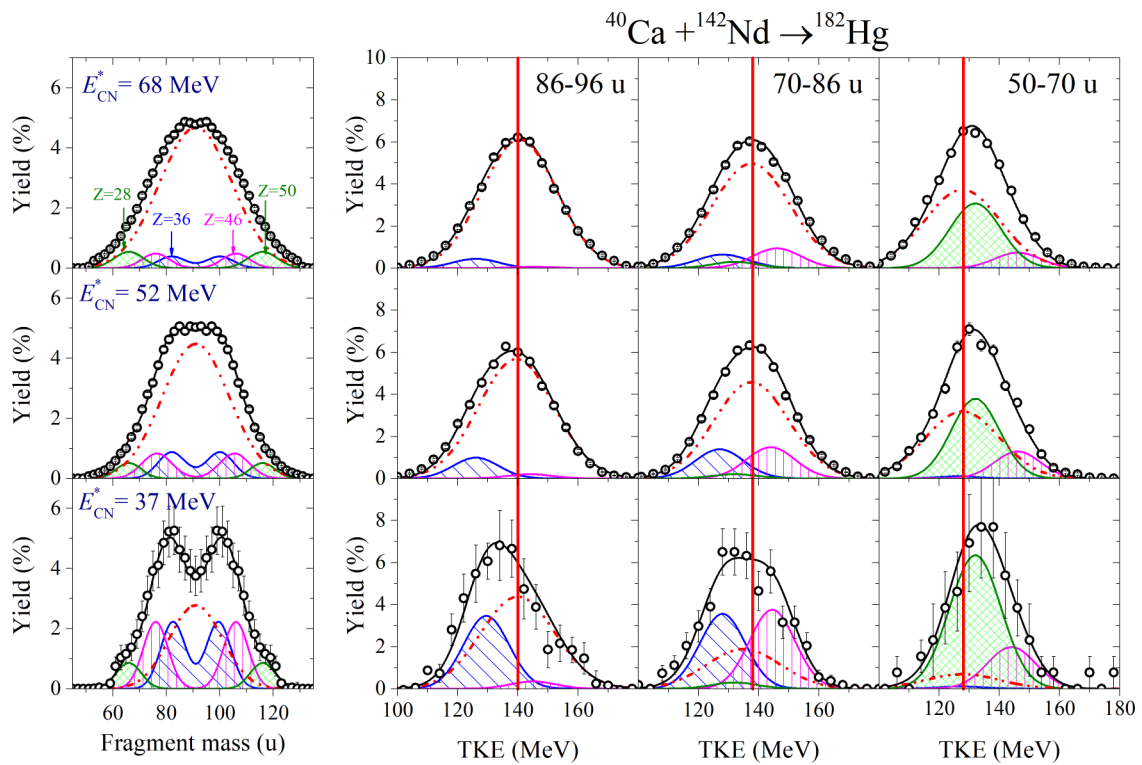
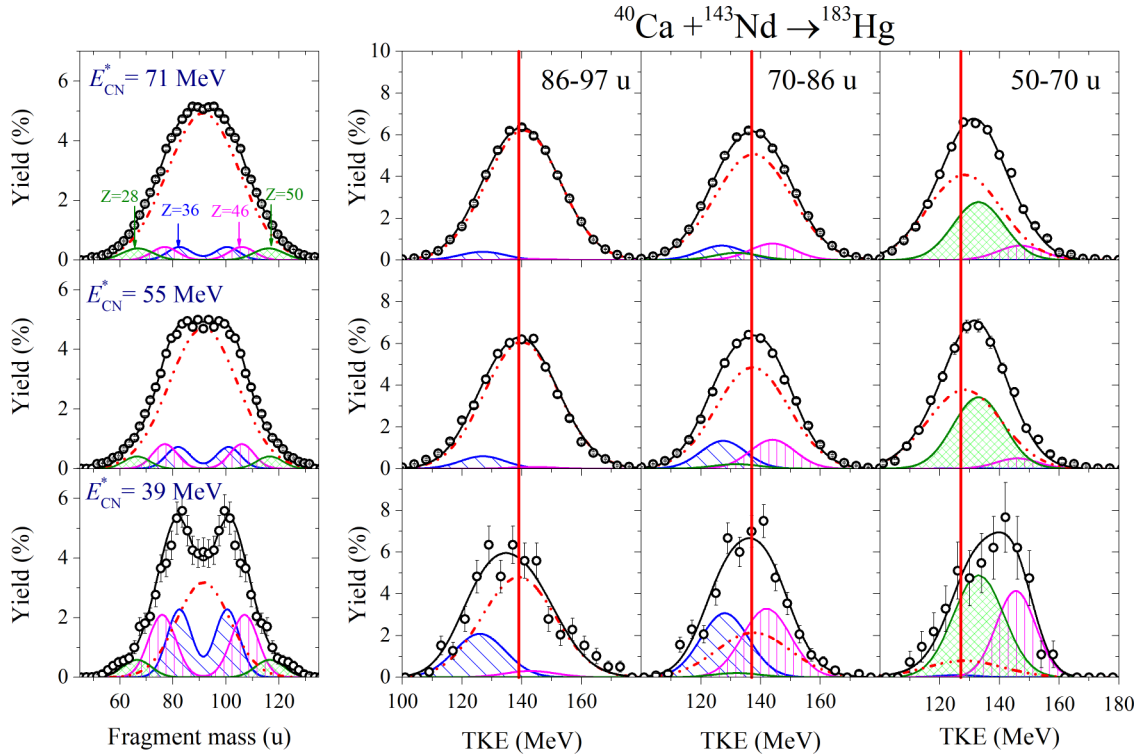


FIG. 2. The mass yields and TKE distributions of fission fragments for different mass regions obtained in the  $^{36}\text{Ar} + ^{144}\text{Sm} \rightarrow ^{180}\text{Hg}$  reaction. The lines correspond to the decompositions of TKE distributions into the symmetric (dashed-dot-dot lines), the asymmetric A1 (diagonally hatched region), the asymmetric A2 (vertically hatched region), and the asymmetric A3 (crosswise hatched region). The vertical lines in the TKE panels indicate the TKE value estimated using the Viola systematics [34]. The half widths at half maximum (HWHM) of experimental distributions are indicated in the TKE panels.

FIG. 3. The same as in Fig. 2 but for the  $^{36}\text{Ar} + ^{142}\text{Nd}$  reaction.FIG. 4. The same as in Fig. 2 but for the  $^{40}\text{Ca} + ^{142}\text{Nd}$  reaction.

FIG. 5. The same as in Fig. 2 but for the  $^{40}\text{Ca} + ^{143}\text{Nd}$  reaction.

plex structure and change significantly with fragment mass. Several components with vastly different mean energies are clearly visible.

Let us consider the peculiarities of the fission fragments mass and energy distributions by the example of  $^{180}\text{Hg}$  (see Fig. 2). According to the LDM, the TKE of fission fragments does not depend on the CN excitation energy and has a parabolic dependence on fragment mass,

$$\text{TKE}(M) = 4 \text{TKE}_{\text{Viola}} \frac{M(A_{\text{CN}} - M)}{A_{\text{CN}}^2},$$

where  $M$  is a fragment mass and  $\text{TKE}_{\text{Viola}}$  is the most probable TKE estimated using the Viola systematics [34]. The vertical red lines in the TKE panels of Fig. 2 indicate the expected TKE values for symmetric mode for given fragment mass range.

Systematic study of mass and energy distributions of fission fragments of excited nuclei [33] showed that for the nuclei with  $Z^2/A^{1/3} \approx 1100$ , the standard deviation of TKE distribution amounts about 9.5–10 MeV. Taking into account energy resolution of the present measurements, we can expect the standard deviation of TKE distribution for the symmetric mode to be of about 11 MeV.

It is obvious from Fig. 2 that the measured TKE distributions deviate from a single Gaussian shape expected from the LDM. This is manifested the most clearly at the lowest excitation energy (34 MeV). In this case, for the symmetric mass split (the left bottom TKE panel in Fig. 2) the narrow component with the mean energy of about 129 MeV (that is considerably lower than the TKE expected for symmetric mode according to the LDM) is seen. The HWHM of this

narrow component is about 10 MeV ( $\sigma \approx 8.5$  MeV in terms of standard deviation). The wide component (HWHM  $\approx 13$  MeV,  $\sigma \approx 11$  MeV) centered at the energy of about 142 MeV that is close to the value estimated using Viola systematics (vertical red line) is also seen in this distribution. The standard deviation of this wide component is consistent with the expectation for symmetric fission, whereas the low-energy component has smaller variance. Note, that the study of modal fission of actinides [39] showed that the variance of TKE distributions for asymmetric modes caused by the shell effects is smaller than for the symmetric LDM mode. Strong deviation of properties observed for the low-energy component from the expectations for the symmetric mode gives us a reason to introduce the A1 asymmetric mode (blue diagonally hatched region).

At the same time, for more asymmetric fission configurations (the middle bottom TKE panel in Fig. 2), together with the low-energy peak at  $\text{TKE} \approx 129$  MeV, the second maximum in the experimental distribution is observed at  $\text{TKE} \approx 145$  MeV that is about 5 MeV above the most probable value expected for the symmetric mode at this mass range. The width of this high-energy component is smaller (HWHM  $\approx 9$ ,  $\sigma \approx 7.3$  MeV) than the one expected for the symmetric mode. This gives us a clear reason to involve one more asymmetric mode A2 (magenta vertically hatched region).

And finally, for very asymmetric fission configurations (50–70 u) (the right bottom TKE panel in Fig. 2), the maximum of the experimental TKE distribution is about 3 MeV higher than the TKE for the symmetric LDM mode. Moreover, the distribution is narrower (HWHM  $\approx 10$ ,  $\sigma \approx 8.5$  MeV) than expected from the LDM. In this mass region, the numbers

of protons in the fission fragments are close to the proton shells at  $Z = 28$  and  $50$ . Note that in the fission of actinide nuclei, the asymmetric mode caused by the proton shell at  $Z \approx 52$  manifests itself [4]. We may expect that this shell also affects the formation of preactinide fission fragments especially because, in this case, the complementary light fragments are close to the proton shell at  $Z = 28$ . Therefore, the introduction of the third asymmetric mode A3 (green cross-wise hatched region) seems to be quite reasonable.

With increasing the excitation energy, the component associated with the LDM becomes dominant. As seen from Figs. 3–5 the behavior of the mass and energy distributions of the  $^{182,183}\text{Hg}$  and  $^{178}\text{Pt}$  fission fragments is similar to  $^{180}\text{Hg}$ .

Thus, the trends in TKE allow us to assume the existence of one symmetric ( $S$ ) and three asymmetric modes (A1, A2, and A3) in the fission of preactinide nuclei. The A1 mode is connected with nearly symmetric low-energy fragments, the A2 mode—with high-energy fragments in the light mass range of 70–85 u, and the A3 mode appears for asymmetric fragments with light fragment masses of 50–70 u.

The symmetric  $S$  mode showing the TKE value, consistent to the Viola systematics within the experimental uncertainties, is attributed to the LDM valley. At the fitting procedure of mass distributions, we used the empirical systematics based on the LDM [33] to fix the variance of the  $S$  mode. The widths of Gaussians corresponding to the asymmetric fission modes varied in the range of 3.5–5 u depending on the CN excitation energy. They are close to those (4 u) found for the asymmetric mass distribution of  $^{180}\text{Hg}$  from the  $\beta$ -delayed fission of  $^{180}\text{Tl}$ . The positions and yields of asymmetric modes were adjusted to agree with the decompositions of TKE distributions, i.e., to make the contributions of each mode in mass distributions equal to those in TKE ones. The decompositions of the mass and energy distributions into the  $S$ , A1, A2, and A3 modes are shown in Figs. 2–5. The deduced values of the most probable masses and TKEs for each mode are listed in Table II. The proton and neutron numbers were estimated based on UCD assumption [25]. The pre-scission neutron evaporation may add uncertainties to the obtained proton and neutron numbers of about 0.4 u. Moreover, the experimental resolution of our mass measurements is about  $\pm 2$  u. For these reasons, we estimate the accuracy of proton and neutron numbers for the A1, A2, and A3 modes found at the fitting procedure of mass distributions as  $\pm 1$  u. The accuracy of the obtained TKE values is  $\pm 2$  MeV including the statistical and the systematic errors of measurements.

Although the studied CNs have nearly the same number of protons as well as of neutrons, the difference in fission fragment proton and neutron numbers was observed (see Table II). The near constant proton numbers for all studied nuclei are found to be  $Z_L \approx 36$  in the light fragment for the A1 mode,  $Z_H \approx 46$  in the heavy fragment for the A2 mode, and  $Z_L \approx 28$  in the light and  $Z_H \approx 50$  in the heavy fragment for the A3 mode. Since the kinetic energy of fragments originates mainly from the Coulomb repulsion at the scission point, the TKE value depends on the distance  $d$  between the centers of the formed fragments. It allows us to estimate the shape at scission for various modes: the A2 mode is more compact than

TABLE II. The masses ( $M_{L,H}$ ), the proton ( $Z_{L,H}$ ), and neutron ( $N_{L,H}$ ) numbers of the light and the heavy fragments and the TKEs of the symmetric ( $S$ ) and the asymmetric (A1, A2, and A3) fission modes for the studied CNs. The proton and neutron numbers were deduced based on the UCD hypothesis.

CN	Mode	$M_L$ u	$M_H$ u	$Z_L$	$Z_H$	$N_L$	$N_H$	TKE MeV
$^{178}\text{Pt}$	$S$	89		39		50		136
	A1	82.5	95.5	36.2	41.8	46.3	53.7	125
	A2	73.5	104.5	32.2	45.8	41.3	58.7	140
	A3	64.0	114.0	28.0	50.0	36.0	64.0	127
$^{180}\text{Hg}$	$S$	90		40		50		142
	A1	81.0	99.0	36.0	44.0	45.0	55.0	127
	A2	76.5	103.5	34.0	46.0	42.5	57.5	145
	A3	65.8	114.3	29.2	50.8	36.5	63.5	132
$^{182}\text{Hg}$	$S$	91		40		51		140
	A1	82.5	99.5	36.3	43.7	46.2	55.8	128
	A2	76.5	105.5	33.6	46.4	42.9	59.1	144
	A3	66.0	116.0	29.0	51.0	37.0	65.0	132
$^{183}\text{Hg}$	$S$	91.5		40		51.5		139
	A1	82.5	100.5	36.1	43.9	46.4	56.6	128
	A2	77.0	106.0	33.7	46.3	43.3	59.7	145
	A3	66.5	116.5	29.1	50.9	37.4	65.6	133

the LDM one, whereas for the A1 mode, the shape is more elongated.

Recently, it was found that the symmetric scission in the light thorium isotopes shows a compact configuration [40]. This new main symmetric scission mode is characterized by a significant drop in deformation energy of the fission fragments of about 19 MeV, compared to the well-known symmetric scission in the uranium plutonium region. In the symmetric fission of Th, the number of protons in the formed fragments is  $Z = 45$  that corresponds to the compact A2 mode. Hence, we may expect that the A2 mode manifests itself in the fission of preactinides as well as actinides.

The TKE value for the A1 mode connected with stabilizing proton number  $Z_L \approx 36$  found in the present paper indicates the well-elongated configuration. The unexpected dominant role of well-deformed proton subsystem with  $Z < 40$  found from the analysis of fragment neutron multiplicities for  $^{178}\text{Hg}$  in Ref. [19] supports the existence of this mode.

The A3 mode introduced for fragments with  $Z = 28$  and  $Z = 50$  may be related to the standard I mode at  $Z \approx 52$  known in the fission of actinide nuclei [3,4].

## B. Fission of $^{178}\text{Pt}$

As was mentioned above, the  $^{36}\text{Ar} + ^{142}\text{Nd}$  reaction leading to  $^{178}\text{Pt}^*$  at similar excitation energies has been studied recently by Tsekhanovich *et al.* [17]. The mass distributions obtained in Ref. [17] together with our data are shown in the left panels of Fig. 6.

The mass distributions obtained in present paper agree within the statistical error and mass resolution with the data from Ref. [17]. The TKE distribution at the excitation energy of 51 MeV reported in Ref. [17] is shown in the right middle

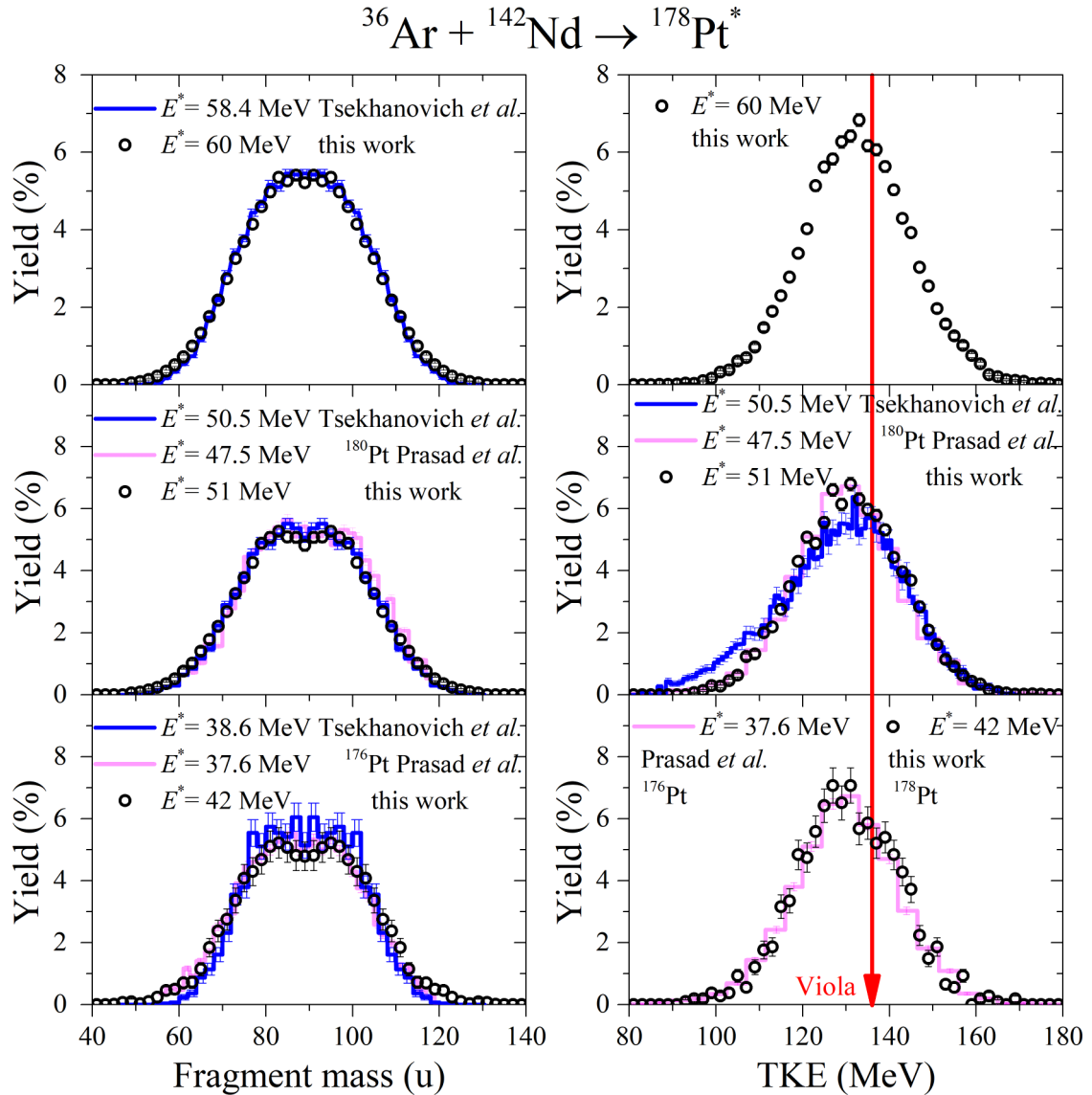


FIG. 6. The mass and TKE distributions of  $^{178}\text{Pt}$  fission fragments obtained in the  $^{36}\text{Ar} + ^{142}\text{Nd}$  reaction in the present paper (open circles) and in Ref. [17] (blue histograms). The mass and TKE distributions of  $^{176,180}\text{Pt}$  fission fragments formed in the  $^{32}\text{S} + ^{144,148}\text{Sm}$  reactions from Ref. [16] are presented by light magenta histograms. The red arrow in the right panel indicates the TKE value obtained from the Viola systematics [34] for  $^{178}\text{Pt}$ .

panel in Fig. 6. It is clearly seen that it is wider than the one measured in this paper and shows an enhanced yield at energies lower than 115 MeV.

The fission of the neighboring  $^{176}\text{Pt}^*$  and  $^{180}\text{Pt}^*$  isotopes via the  $^{32}\text{S} + ^{144,148}\text{Sm}$  fusion reactions was studied by Prasad *et al.* [16]. The mass and energy distributions from Ref. [16] are also presented in Fig. 6 for comparison. As seen from Fig. 6 (bottom and middle panels), the mass and TKE distributions obtained in this paper for  $^{178}\text{Pt}$  and the ones for  $^{176,180}\text{Pt}$  from Ref. [16] are in good agreement taking into account the difference in mass of the fissioning isotopes. No evidence for the low-energy component in TKE distributions was observed, unlike the 30% contribution seen in Ref. [17] for  $^{178}\text{Pt}$ .

Since the yield of asymmetric fission increases with decreasing the CN excitation energy, we analyzed the  $^{178}\text{Pt}$  fission fragments mass distributions, measured in the present

experiment, for the low and the high TKE ranges at the lowest energy  $E^* = 42$  MeV. In Fig. 7, the mass distributions for  $\text{TKE} > 136$  and  $\text{TKE} < 130$  MeV are shown. The low-energy cut differs from the one applied in Ref. [17] ( $\text{TKE} < 114$  MeV) since we did not observe the low-energy tail revealed in Ref. [17]. It is clearly seen that they differ significantly. For the high TKEs, two-humped mass distribution with maxima near 78 and 100 u for the light and the heavy fragments is observed similar to Ref. [17]. For the low TKEs, the mass distribution is more symmetric than for the high TKE, but the structure around masses 83 and 95 u is found. This structure was not seen in Ref. [17] that may be explained by the lower excitation energy of  $^{178}\text{Pt}$  and better mass ( $\pm 2$  u versus  $\pm 4$  u) and energy resolutions in the present experiment.

In accordance with our multicomponent analysis described above, the peculiarities found in mass distributions agree well



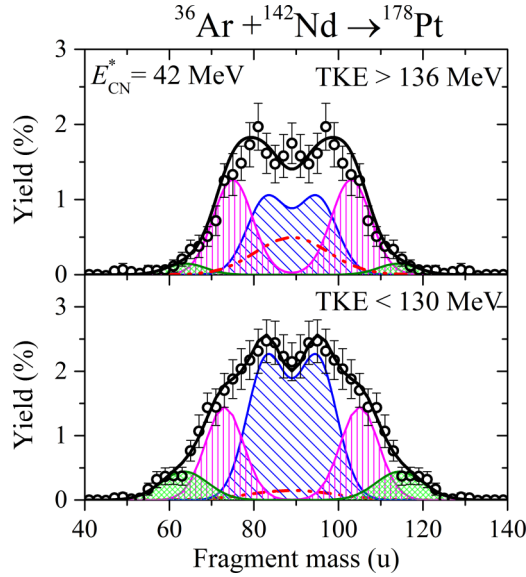


FIG. 7. The  $^{178}\text{Pt}$  fission fragments mass yields for TKE > 136 (top) and for TKE < 130 MeV (bottom) at the excitation energy of 42 MeV. The lines correspond to the decompositions into the symmetric (dashed-dot-dot lines) and the asymmetric A1 (diagonally hatched region), A2 (vertically hatched region), and A3 (crosswise hatched region) modes.

with the manifestation of the A1 and A2 modes in dependence on fission fragment kinetic energy. The ratio between the contribution of the A1 and A2 modes in mass distribution (see Fig. 3) at this excitation energy is about 1.4. Taking into account the most probable TKE values for these modes, we may expect that the contribution of the high-energy A2 mode in mass distribution with TKE > 136 MeV will be larger than that of A1, whereas for TKE < 130 MeV, the opposite behavior is reasonable. Although the most probable TKE values differ considerably for the A1 and A2 modes (see Table II), their standard deviations are about 7–8 MeV that leads to the overlapping of these modes in TKE distribution. As seen from Fig. 3, the low-energy mode A1 reaches the TKE of about 145 MeV, whereas the high-energy mode A2 starts to appear at TKE of about 120 MeV. Thus, the applied gates on fragment TKEs only allow to inhibit the contributions of A1 in the TKE > 136-MeV diapason and A2 in the TKE < 130-MeV one, but not exclude the modes completely.

The decompositions of mass distributions for the low and the high TKE ranges into the S, A1, A2, and A3 modes are presented in Fig. 7. To describe the S mode, we calculated two-dimensional  $M$ -TKE distribution based on LDM (Gaussian mass and energy distributions with parabolic dependence of average TKE on fragment mass) and gated it on TKE in the same manner as the experimental one. The projections on the mass axis were then used in the fitting procedure. The yields of the A1, A2, and A3 modes were varied to obtain the best fit. The deduced ratios between the A1 and A2 modes are 0.8 and 1.6 for TKE > 136 and TKE < 130 MeV, respectively. Thus, the contribution of the A1 mode is larger for the low-energy fragments and smaller for the high-energy ones as opposed for the A2 mode. The structure observed around the masses

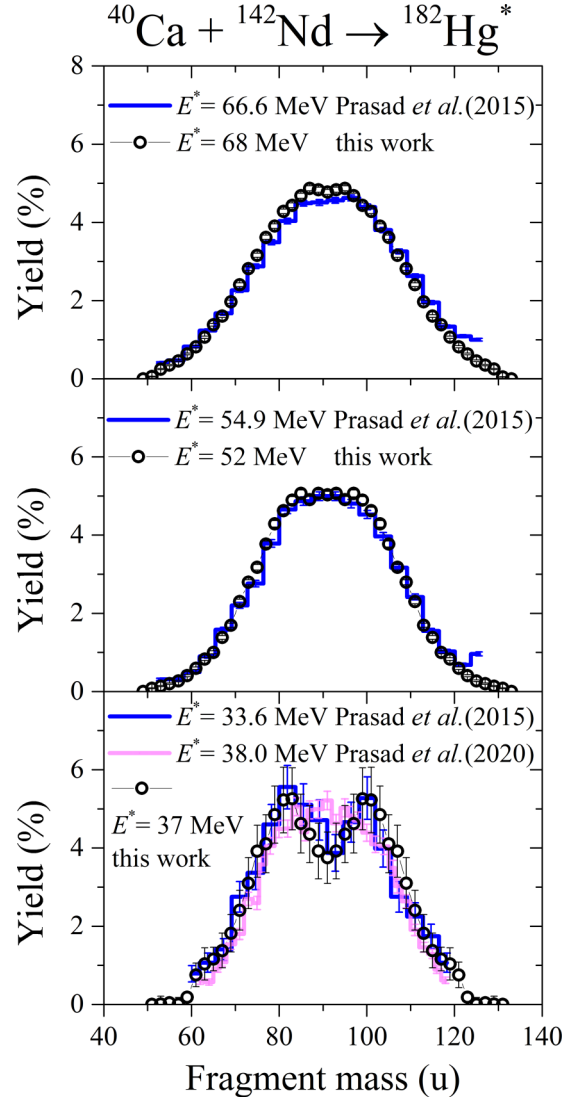


FIG. 8. The  $^{182}\text{Hg}^*$  fission fragments mass distributions obtained in the present paper (open circles) and in Refs. [15,16] (histograms).

83 and 95 u in mass distribution for TKE < 130 MeV coincides with the most probable mass for A1 mode. For TKE > 136 MeV, the contribution of A1 mode is suppressed, but it is still significant, and the maxima near 78 and 100 u correspond to the superposition of the A1 and A2 modes. Consequently, the analyses based on mass gating of TKE distributions and TKE gating of mass distributions are consistent with each other that proves the existence of several asymmetric modes in fission of sublead region.

### C. Comparison of mass and energy distributions of the $^{182,183}\text{Hg}$ fission fragments

Fission of  $^{182}\text{Hg}$  formed in the same  $^{40}\text{Ca} + ^{142}\text{Nd}$  reaction at similar interaction energies was studied by Prasad and co-workers [15,16]. As seen from Fig. 8, the mass yields obtained in this paper agree well with the ones from Ref. [15] at all measured energies and show the pronounced asymmetric shape at the lowest excitation energy (37 MeV in our

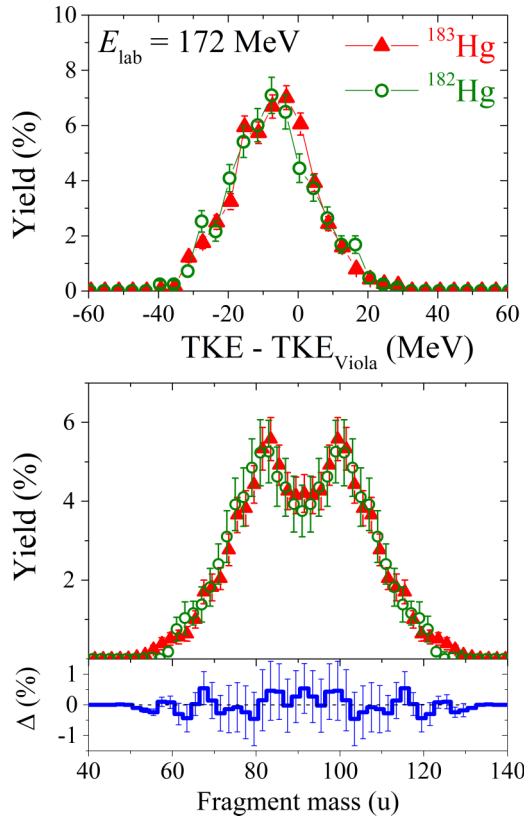


FIG. 9. The TKE distributions (top panel), mass yields (middle panel), and the difference between them (bottom panel) of the  $^{182,183}\text{Hg}$  fission fragments.

measurements and 33.6 MeV in Ref. [15]). The mass distributions in Refs. [15,16] change sharply from asymmetric shape at  $E^* = 33.6$  MeV to nearly symmetric at 38 MeV. The mass distribution measured in the present paper at the excitation energy of 37 MeV has a pronounced asymmetric shape similar to the one of Prasad and co-workers at  $E^* = 33.6$  MeV. It should be noted that in Refs. [15,16], the velocities of fission fragments were deduced from the measured time difference ( $\Delta t$ ) between two detected fission fragments, whereas we measured the ToF of two fragments independently. In both approaches, mass resolution is proportional to the time resolution of the spectrometer. In the case of  $\Delta t$  measurements the mass resolution is better for asymmetric fragments than for symmetric ones, whereas for ToF-ToF measurements, the best resolution is achieved at the symmetric mass split. Probably, the worse mass resolution in the symmetric mass range in Ref. [16] leads to a more symmetric shape of mass distribution at excitation energy of 38 MeV compared to the present measurements.

Besides, the fact that neutron-deficient Hg nuclei undergo the new type of asymmetric fission, a strong difference in shape (shape staggering) of  $^{181,183,185}\text{Hg}$  compared to their even-mass neighbors is a unique feature of these isotopes [28]. The ground-state deformation is strongly prolate ( $(\beta^2)^{1/2} \approx 0.3$ ) for odd-even nuclei, whereas for even-even isotopes it is weakly oblate ( $(\beta^2)^{1/2} \approx 0.2$ ). A question arises if the addition of one extra neutron may influence the fission

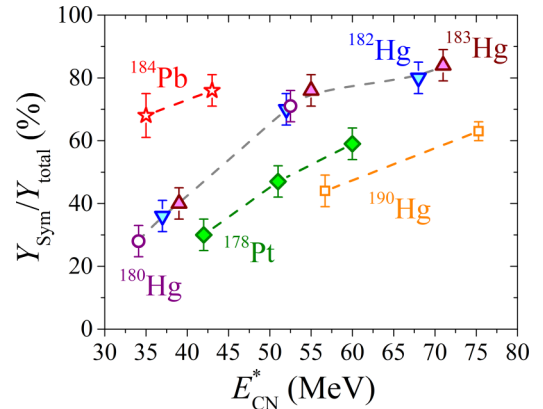


FIG. 10. The contribution of symmetric fission for platinum, mercury, and lead isotopes in dependence on the initial CN excitation energy.

properties of the odd-even Hg nuclei compared to the even-even neighbors.

Of course, in our study, the formed CNs have relatively large excitation energies and angular momenta. It should be noted that the saddle-point deformation of these nuclei is significantly larger ( $\beta_2 \approx 1.4$ ) [41] than their deformation in the ground state. We compared the mass and energy distributions of  $^{182}\text{Hg}$  and  $^{183}\text{Hg}$  fission fragments measured at energy below the Coulomb barrier of the reactions in order to reach the lowest possible excitation energy (about 37–39 MeV) and introduced angular momentum (about  $8 \hbar$ ). The TKE and mass distributions of the  $^{182,183}\text{Hg}$  fission fragments are shown in Fig. 9. The difference between the yields is close to zero within the error bars (see bottom panel of Fig. 9). Thus, in the fission of excited neutron-deficient Hg isotopes, an additional odd neutron does not affect the mass and energy distributions.

#### D. Symmetric mode in the fission of $^{180,182,183,190}\text{Hg}$ , $^{178}\text{Pt}$ , and $^{184}\text{Pb}$

The dependence of the ratio of the symmetric component contribution to the total yield of fission fragments for  $^{180,182,183}\text{Hg}$  and  $^{178}\text{Pt}$  on the initial CN excitation energy is shown in Fig. 10. Also, the yields of the  $S$  mode for  $^{184}\text{Pb}$  and  $^{190}\text{Hg}$ , estimated in Ref. [27] are shown for comparison. For all nuclei, the yield of symmetric fission increases with increasing excitation energy. The contributions of the  $S$  mode are the same within the error bars for  $^{180,182,183}\text{Hg}$ . In the case of  $^{178}\text{Pt}$  (two protons less than Hg) the contribution of the  $S$  mode is lower than that for  $^{180,182,183}\text{Hg}$ , whereas for  $^{184}\text{Pb}$  (two protons more than Hg) it is significantly larger at the saddle-point energies below 30 MeV ( $E_{\text{CN}}^*$  lower than 50 MeV, see Table I). Note that both  $^{178}\text{Pt}$  and  $^{184}\text{Pb}$  have nearly the same number of neutrons as  $^{180,182,183}\text{Hg}$ . On the other hand, the yield of symmetric fission for  $^{190}\text{Hg}$  is slightly lower than for  $^{180,182,183}\text{Hg}$  and close to  $^{178}\text{Pt}$  at the same excitation energies of CN at the saddle point. At energies above 30 MeV, the pre-scission emission may affect the fission properties of these nuclei.

#### IV. CONCLUSIONS

To investigate the dependence of the symmetric and asymmetric fission of preactinide nuclei on the excitation energy and neutron numbers of CNs, the fission fragments mass-energy distributions of  $^{180,182,183}\text{Hg}$  and  $^{178}\text{Pt}$  formed in the  $^{36}\text{Ar} + ^{144}\text{Sm}$ ,  $^{40}\text{Ca} + ^{142,143}\text{Nd}$ , and  $^{36}\text{Ar} + ^{142}\text{Nd}$  reactions were measured using the double-arm time-of-flight spectrometer CORSET.

The observed peculiarities in TKE distributions from the fission of  $^{178}\text{Pt}$  and  $^{180,182,183}\text{Hg}$  may be interpreted as a superposition of one symmetric LDM component and three asymmetric modes, namely, the low-energy one for nearly symmetric fragments, the high-energy for more asymmetric fragments (70–85 u for light fragments), and the midenergy one for light fragments with masses 50–70 u. For all studied nuclei, the decompositions of the mass and TKE distributions into symmetric, associated with LDM, and three asymmetric fission modes were performed. The stabilizing role of proton number  $Z \approx 36$  in the light fragment,  $Z \approx 46$  in the heavy fragment, and  $Z = 28$  and/or 50 in both the light and the heavy fragments was deduced from the analysis of mass and energy distributions of  $^{180,182,183}\text{Hg}$  and  $^{178}\text{Pt}$ .

In the case of the mode determined by the proton number  $Z \approx 36$ , the shape of the fissioning nucleus is more elongated than LDM prediction and more compact for the mode connected with  $Z \approx 46$ . Thus, in the fission of neutron-deficient sublead nuclei the strongly deformed proton shell at  $Z \approx 36$  and the weakly deformed one at  $Z \approx 46$  are found to be responsible for the new type of asymmetric fission.

At the saddle-point excitation energy below 30 MeV when the pre-scission emission is negligible, the yield of the symmetric component, linked to LDM, grows with the increasing proton number of CN. For neutron-deficient nuclei with  $N \approx 100$ , the contribution of the mode is about 65% for  $^{184}\text{Pb}$ , about 40% for  $^{180,182,183}\text{Hg}$ , and about 35% for  $^{178}\text{Pt}$ . The contributions of the symmetric mode for  $^{180,182,183}\text{Hg}$  are, within the error bars, the same. In the case of  $^{178}\text{Pt}$  it is slightly lower. The yields of this component increase with the excitation energy for all studied nuclei.

A comparison of mass and energy distributions of the  $^{183}\text{Hg}^*$  and  $^{182}\text{Hg}^*$  fission fragments showed that the addition of one odd neutron does not affect their properties, regardless that it leads to a dramatic change in the ground-state deformations of these isotopes.

#### ACKNOWLEDGMENTS

We thank the FLNR accelerator team for excellent beam quality, smooth operation of the cyclotron throughout the experiment, and a friendly and professional attitude. Strong support of the directorate of the FLNR JINR is greatly acknowledged. This work was supported by the joint Grant from the Russian Foundation for Basic Research (Grant No. 19-52-45023) and the Department of Science and Technology of the Ministry of Science and Technology of India (Grant No. INT/RUS/RFBR/387). A.N.A. was supported by the Grant from STFC (UK).

- 
- [1] M. G. Itkis, N. A. Kondrat'ev, Yu. V. Kotlov, S. I. Mul'gin, V. N. Okolovich, A. Ya. Rusanov, and G. N. Smirenkin, *Sov. J. Nucl. Phys.* **47**, 4 (1988).
- [2] A. N. Andreyev, J. Elseviers, M. Huyse, P. Van Duppen, S. Antalic, A. Barzakh *et al.*, *Phys. Rev. Lett.* **105**, 252502 (2010).
- [3] K.-H. Schmidt, S. Steinhäuser, C. Böckstiegel, A. Grewe, A. Heinz, A. R. Junghans *et al.*, *Nucl. Phys. A* **665**, 221 (2000).
- [4] C. Böckstiegel, S. Steinhäuser, K.-H. Schmidt, H.-G. Clerc, A. Grewe, A. Heinz, M. de Jong, A. R. Junghans, J. Müller, and B. Voss, *Nucl. Phys. A* **802**, 12 (2008).
- [5] P. Möller, J. Randrup, and A. J. Sierk, *Phys. Rev. C* **85**, 024306 (2012).
- [6] T. Ichikawa, A. Iwamoto, P. Möller, and A. J. Sierk, *Phys. Rev. C* **86**, 024610 (2012).
- [7] G. Scamps and C. Simenel, *Phys. Rev. C* **100**, 041602(R) (2019).
- [8] J. D. McDonnell, W. Nazarewicz, J. A. Sheikh, A. Staszczak, and M. Warda, *Phys. Rev. C* **90**, 021302(R) (2014).
- [9] A. V. Andreev, G. G. Adamian, and N. V. Antonenko, *Phys. Rev. C* **86**, 044315 (2012).
- [10] A. V. Andreev, G. G. Adamian, N. V. Antonenko, and A. N. Andreyev, *Phys. Rev. C* **88**, 047604 (2013).
- [11] H. Pasca, A. V. Andreev, G. G. Adamian, and N. V. Antonenko, *Phys. Rev. C* **101**, 064604 (2020).
- [12] S. Panebianco, J.-L. Sida, H. Goutte, J.-F. Lemaître, N. Dubray, and S. Hilaire, *Phys. Rev. C* **86**, 064601 (2012).
- [13] K. Nishio, A. N. Andreyev, R. Chapman, X. Derkx, Ch. E. Düllmann, L. Ghys *et al.*, *Phys. Lett. B* **748**, 89 (2015).
- [14] R. Tripathi, S. Sodaye, K. Sudarshan, B. K. Nayak, A. Jhingan, P. K. Pujari, K. Mahata, S. Santra, A. Saxena, E. T. Mirgule, and R. G. Thomas, *Phys. Rev. C* **92**, 024610 (2015).
- [15] E. Prasad, D. J. Hinde, K. Ramachandran, E. Williams, M. Dasgupta, I. P. Carter, K. J. Cook, D. Y. Jeung, D. H. Luong, S. McNeil, C. S. Palshetkar, D. C. Rafferty, C. Simenel, A. Wakhle, J. Khuyagbaatar, Ch. E. Düllmann, B. Lommel, and B. Kindler, *Phys. Rev. C* **91**, 064605 (2015).
- [16] E. Prasad, D. J. Hinde, M. Dasgupta, D. Y. Jeung, A. C. Berriman, B. M. A. Swinton-Bland *et al.*, *Phys. Lett. B* **811**, 135941 (2020).
- [17] I. Tsekhanovich, A. N. Andreyev, K. Nishio, D. Denis-Petit, K. Hirose, H. Makii *et al.*, *Phys. Lett. B* **790**, 583 (2019).
- [18] B. M. A. Swinton-Bland, M. A. Stoyer, A. C. Berriman, D. J. Hinde, C. Simenel, J. Buete, T. Tanaka, K. Banerjee, L. T. Bezzina, I. P. Carter, K. J. Cook, M. Dasgupta, D. Y. Jeung, C. Sengupta, E. C. Simpson, and K. Vo-Phuoc, *Phys. Rev. C* **102**, 054611 (2020).
- [19] C. Schmitt, A. Lemasson, K.-H. Schmidt, A. Jhingan, S. Biswas, Y. H. Kim, D. Ramos, A. N. Andreyev, D. Curien, M. Ciemala, E. Clément, O. Dorvaux, B. De Canditiis, F. Didierjean, G. Duchêne, J. Dudouet, J. Frankland, B. Jacquot, C. Raison, D. Ralet, B.-M. Retaillé, L. Stuttgé, and I. Tsekhanovich, *Phys. Rev. Lett.* **126**, 132502 (2021).

- [20] E. M. Kozulin, E. Vardaci, W. H. Trzaska, A. A. Bogachev, I. M. Itkis, A. V. Karpov, G. N. Knyazheva, and K. V. Novikov, *Phys. Lett. B* **819**, 136442 (2021).
- [21] M. Warda, A. Staszczak, and W. Nazarewicz, *Phys. Rev. C* **86**, 024601 (2012).
- [22] A. V. Andreev, G. G. Adamian, and N. V. Antonenko, *Phys. Rev. C* **93**, 034620 (2016).
- [23] J.-F. Lemaître, S. Goriely, S. Hilaire, and J.-L. Sida, *Phys. Rev. C* **99**, 034612 (2019).
- [24] T. Ichikawa and P. Möller, *Phys. Lett. B* **789**, 679 (2019).
- [25] R. Vandebosch and J. R. Huizenga, *Nuclear Fission* (Academic Press, New York, 1973).
- [26] K. Mahata, C. Schmitt, S. Gupta, A. Shrivastava, G. Scamps, and K.-H. Schmidt, [arXiv:2007.16184](https://arxiv.org/abs/2007.16184).
- [27] A. A. Bogachev, E. M. Kozulin, G. N. Knyazheva, I. M. Itkis, M. G. Itkis, K. V. Novikov, D. Kumar, T. Banerjee, I. N. Diatlov, M. Cheralu, V. V. Kirakosyan, Y. S. Mukhamejanov, A. N. Pan, I. V. Pchelintsev, R. S. Tikhomirov, I. V. Vorobiev, M. Maiti, R. Prajapat, R. Kumar, G. Sarkar, W. H. Trzaska, A. N. Andreyev, I. M. Harca, and E. Vardaci, *Phys. Rev. C* **104**, 024623 (2021).
- [28] B. A. Marsh, T. Day Goodacre, S. Sels, Y. Tsunoda, B. Andel, A. N. Andreyev *et al.*, *Nat. Phys.* **14**, 1163 (2018).
- [29] E. M. Kozulin, A. A. Bogachev, M. G. Itkis, I. M. Itkis, G. N. Knyazheva, N. A. Kondratiev *et al.*, *Instrum. Exp. Tech.* **51**, 44 (2008).
- [30] D. J. Hinde, M. Dasgupta, J. R. Leigh, J. C. Mein, C. R. Morton, J. O. Newton, and H. Timmers, *Phys. Rev. C* **53**, 1290 (1996).
- [31] R. Bass, *Nucl. Phys. A* **231**, 45 (1974).
- [32] A. J. Sierk, *Phys. Rev. C* **33**, 2039 (1986).
- [33] M. G. Itkis and A. Ya. Rusanov, *Phys. Part. Nucl.* **29**, 160 (1998).
- [34] V. E. Viola, K. Kwiatkowski, and M. Walker, *Phys. Rev. C* **31**, 1550 (1985).
- [35] D. Hilscher and H. Rossner, *Ann. Phys. France* **17**, 471 (1992).
- [36] A. V. Karpov, A. S. Denikin, M. A. Naumenko, A. P. Alekseev, V. A. Rachkov, V. V. Samarín, V. V. Saiko, and V. I. Zagrebaev, *Nucl. Instrum. Methods Phys. Res. Sect. A* **859**, 112 (2017).
- [37] A. Gavron, *Phys. Rev. C* **21**, 230 (1980); O. B. Tarasov and D. Bazin, *Nucl. Instrum. Methods Phys. Res. Sect. B* **266**, 4657 (2008).
- [38] R. du Rietz, E. Williams, D. J. Hinde, M. Dasgupta, M. Evers, C. J. Lin, D. H. Luong, C. Simenel, and A. Wakhle, *Phys. Rev. C* **88**, 054618 (2013).
- [39] S. I. Mulgin, S. V. Zhdanov, N. A. Kondratiev, K. V. Kovalchuk, and A. Ya. Rusanov, *Nucl. Phys. A* **824**, 1 (2009).
- [40] A. Chatillon, J. Taïeb, H. Alvarez-Pol, L. Audouin, Y. Ayyad, G. Bélier, J. Benlliure, G. Boutoux, M. Caamaño, E. Casarejos, D. Cortina-Gil, A. Ebranl, F. Farget, B. Fernández-Domínguez, T. Gorbinet, L. Grente, A. Heinz, H. T. Johansson, B. Jurado, A. Kelić-Heil, N. Kurz, B. Laurentl, J.-F. Martin, C. Nociforo, C. Paradela, E. Pellereau, S. Pietri, A. Prochazka, J. L. Rodríguez-Sánchez, D. Rossi, H. Simon, L. Tassan-Got, J. Vargas, B. Voss, and H. Weick, *Phys. Rev. Lett.* **124**, 202502 (2020).
- [41] S. Cohen, F. Plasil, and W. J. Swiatecki, *Ann. Phys. (NY)* **82**, 557 (1974).